Nanoscale

Accepted Manuscript

Volume 8 | Number 1 | 7 January 2016 | Pages 1–660

Nanoscale

www.rsc.org/nanoscale

ISSN 2040-3364

ROYAL SOCIETY OF CHEMISTRY

PAPER
Qian Wang et al.
Ti₃C₂ a new two-dimensional sheet beyond MXenes

NCNST

ROYAL SOCIETY OF CHEMISTRY

rsc.li/nanoscale

Journal Name

ARTICLE

Fe₃O₄@Au@mSiO₂ as Enhancing Nanoplatform for Rose Bengal Photodynamic Activity

I. Rosa-Pardo,[a] M. Roig-Pons,[a] A. A. Heredia,[a, †] J. V. Usagre,[a] A. Ribera,[a] R. E. Galian[a*] and J. Pérez-Prieto[a*]

A novel nanoplatform composed of three types of materials with different functionalities, specifically core-shell Fe₃O₄@Au nanoparticles encapsulated near the outer surface of mesoporous silica (mSiO₂) nanoparticles, has been successfully synthesised and used to enhance the efficiency of a photosensitiser, namely Rose Bengal, in singlet oxygen generation. The Fe₃O₄ is responsible for the unusual location of the Fe₃O₄@Au nanoparticle, while the plasmonic shell acts as an optical antenna. In addition, the mesoporous silica matrix firmly encapsulates Rose Bengal by chemical bonding inside the pores, thus guaranteeing its photostability, and it makes the nanosystem biocompatible. Moreover, the silica surface of the nanoplatform ensures further functionalisation on demand.

Introduction

The assembling of different materials is of great interest and can be used to build a nanoplatform that combines the individual (photo)physical/(photo)chemical capacities (such as photoluminescence, magnetism, encapsulation, singlet oxygen generation, catalysis, etc.) of the components or, via their synergistic effect, creates a new functionality or enhances that of one of the components. [1-5]

Nanoplatforms containing Fe₃O₄ are promising magnetic-targeted smart drug delivery systems that can increase the concentration of therapeutic drugs at the targeted location, thus avoiding the toxic effect of drugs in healthy cells and tissues due to non-specific uptake. [6]

Curious behaviour has been observed when embedding small Fe₃O₄ nanoparticles (NPs) in mSiO₂ NPs. [7] While silica condensation in the presence of seed magnetic NPs usually yields a core-shell morphology, Fe₃O₄ NPs integrate into mSiO₂ NPs near the outer surface and without disrupting their ordered structure. Transmission electron microscopy (TEM) images showed several embedded Fe₃O₄ NPs accumulated near the outer surface of the silica NP.

[a] ICMOL, Universidad de Valencia, Catedrático José Beltrán 2, 46980, Paterna, Valencia, Spain. Fax: 34 963543576; Tel: 34 963543050

† INFIQC, Facultad de Ciencias Químicas, Universidad Nacional de Córdoba, Ciudad Universitaria, X5000HUA Córdoba, Argentina.

Electronic Supplementary Information (ESI) available: Additional Absorption spectra, microscopy images and experimental details. See DOI: 10.1039/x0xx00000x

Magnetic nanoparticles (Fe₃O₄ NPs) are unstable under physiological conditions and can promote the formation of harmful free radicals. [8-10] The coating of Fe₃O₄ NPs with gold enhances their chemical stability by protecting them from oxidation and corrosion. Integration of Fe₃O₄@Au NPs in a biocompatible porous structure, such as mesoporous SiO₂ (mSiO₂) microspheres has recently been used to mimic an artificial enzymatic cascade. [11]

Moreover, mSiO₂ nanoparticles could be used to increase the local concentration of a drug by making use of the pores of the material. [12] In addition, the large surface area of the nanoparticle can be easily functionalised with targeted molecules by covalent bonding. [13] Furthermore, the gold component of Fe₃O₄@Au NPs can enhance the singlet oxygen generation of the drug (a photosensitiser) at a certain distance from the nanoparticle.

Consequently, we hypothesised that a novel Fe₃O₄@Au@mSiO₂ nanoplatform, (i.e. <100 nm, NPT in Scheme 1) in which a small Fe₃O₄ NP covered by a thin Au shell and integrated near the outer surface of an ordered mSiO₂ NP could be a suitable nanoplatform to enhance the singlet oxygen generation of an encapsulated photosensitiser.

Rose Bengal (RB) is U.S. Food and Drug Administration-approved as a diagnostic agent for ocular surface defects[14] and it has been tested in photoactivated tissue bonding. [15] In addition, RB is an experimental agent for photodynamic therapy treatment. [16] It exhibits intense absorption bands in the visible spectrum (480-550 nm with a peak maximum at

549 nm in water and molar absorption coefficient of around 95,000 dm^{3}mol^{-1}cm^{-1}), low fluorescence quantum yield (0.02 in water), high triplet quantum yield (0.76), long-lived triplet state, and produces singlet oxygen with high quantum yield (around 0.76 in water) [17-19]. The pores of mSiO$_2$ have proved useful for protecting RB from photochemical degradation. [20,21,22]
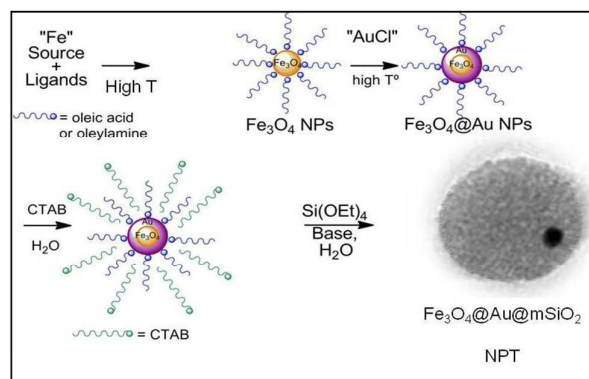
Scheme 1: General procedure for the preparation of the biocompatible and photostable Fe$_3$O$_4$@Au@mSiO$_2$ nanoplatform.

We report here the preparation of a functional nanoplatform (ca. 60 nm), which consists of a small Fe$_3$O$_4$ nanoparticle (around 5 nm) covered by a thin gold shell (2-3 nm), whose synthesis has been optimised by using AuCl as the gold precursor, embedded near the outer surface of mSiO$_2$ and eventually loaded with RB covalently bonded to the silanol groups in the silica pores. Notably, the Fe$_3$O$_4$@Au@mSiO$_2$-RB nanosystem exhibits enhanced capacity for singlet oxygen generation compared to that of not only RB but also mSiO$_2$-RB.

Results and discussion

The Fe$_3$O$_4$@Au core-shell NPs were synthesised using Fe$_3$O$_4$ nanoparticles as the seeds for growing the Au shell by means of reduction of a gold salt (gold acetate [Au(OOCCH$_3$)$_3$], chloroauric acid (HAuCl$_4$), or gold chloride (AuCl)) at a high temperature in the presence of a mild reducing agent (oleylamine). The effect of these salt precursors on the size, sample homogeneity and optical properties of the core-shell nanoparticles (termed Fe$_3$O$_4$@Au-1, Fe$_3$O$_4$@Au-2 and Fe$_3$O$_4$@Au-3 for the nanoparticles arising from Au(OOCCH$_3$)$_3$, HAuCl$_4$, and AuCl, respectively) was analysed by different techniques such as absorption spectroscopy and high resolution transmission electron microscopy (HRTEM). These core-shell nanoparticles were incorporated into mSiO$_2$ in order to provide biocompatibility and allow further functionalisation of the hybrid NPT (Scheme 1). The preparation of NPT is described below.

Preparation of Fe$_3$O$_4$@Au core-shell NPs

First, the synthesis of Fe$_3$O$_4$ NPs was carried out by following a previously reported methodology with slight modifications.[23] In brief, a deaerated solution containing the iron precursor, Fe(III) acetylacetonate [Fe(acac)$_3$], oleylamine, oleic acid and 1,2-hexadecanediol was heated at a high temperature and under vigorous stirring. After 4 hours of reaction the solution was cooled down to room temperature (crude of magnetic NPs). A few millilitres of the crude was separated and washed twice with ethanol in order to obtain a clean sample of magnetic NPs for their characterisation. The rest of the crude was used for the preparation of Fe$_3$O$_4$@Au core-shell NPs.

The Fe$_3$O$_4$ NPs dispersed in toluene showed an unfeatureless absorption spectrum with absorbance decreasing from 300 to 800 nm (Figure S1). The HRTEM images showed the high homogeneity and crystallinity of the nanoparticles with an average diameter of 5.0 ± 0.2 nm (Figure S1). The small size distribution of the magnetic nanoparticle seeds is crucial for the preparation of homogeneous Fe$_3$O$_4$@Au core-shell NPs.

Then, the preparation of the Fe$_3$O$_4$@Au NPs was carried out by thermal reduction of the gold salt on the magnetic NP surface. In brief, 5 mL of the crude sample containing the magnetic NPs, the gold precursor (1.1 mmol), oleic acid, oleylamine and 1,2-hexadecanothiol were mixed in phenyleter. The mixture was heated at 180-190 ^{0}C for 1.5 h (see experimental section for details). The dark purple solution obtained was cooled down to room temperature and centrifuged with ethanol to produce a solid. When using Au(OOCCH$_3$)$_3$ as the gold precursor, an additional centrifugation of the supernatant led to another solid.

The UV-visible absorption spectra in toluene of the core-shell NPs arising from the different Au salt precursors are shown in Figure 1. [24] The surface plasmon band (SPB) peak of the Fe$_3$O$_4$@Au-1 NPs was at 523 nm and 515 nm for the first and second precipitate, respectively. The precipitate obtained from HAuCl$_4$ (Fe$_3$O$_4$@Au-2) and AuCl (Fe$_3$O$_4$@Au-3) presented the surface plasmon peak at 522 and 523 nm, respectively (Figure 1).

The plasmon peak wavelength of Au nanoshells and the relative contributions of absorption and scattering to the total extinction depend on the inner radius of the shell and its thickness.[25-26] The red shift of the plasmon peak increases with the nanoparticle diameter (D) to the shell thickness (r) ratio, i.e., it does not only depend on the shell thickness but also on the size of the core. Thus, it has been reported that in small Fe$_3$O$_4$@Au nanoparticles (6.6 and 6.3 nm in diameter), the peak changes from 550 nm to 535 nm when the D/r ratio decreases from 9.4 to 7.0.[27] In the case of Fe$_3$O$_4$@Au-3, the D/r ratio is only of 3.3 (see D and r data below) and, consequently, the surface plasmon peak of Fe$_3$O$_4$@Au-3 in toluene was at 523 nm, i.e., at a similar wavelength to that of a solid AuNP of a similar size.
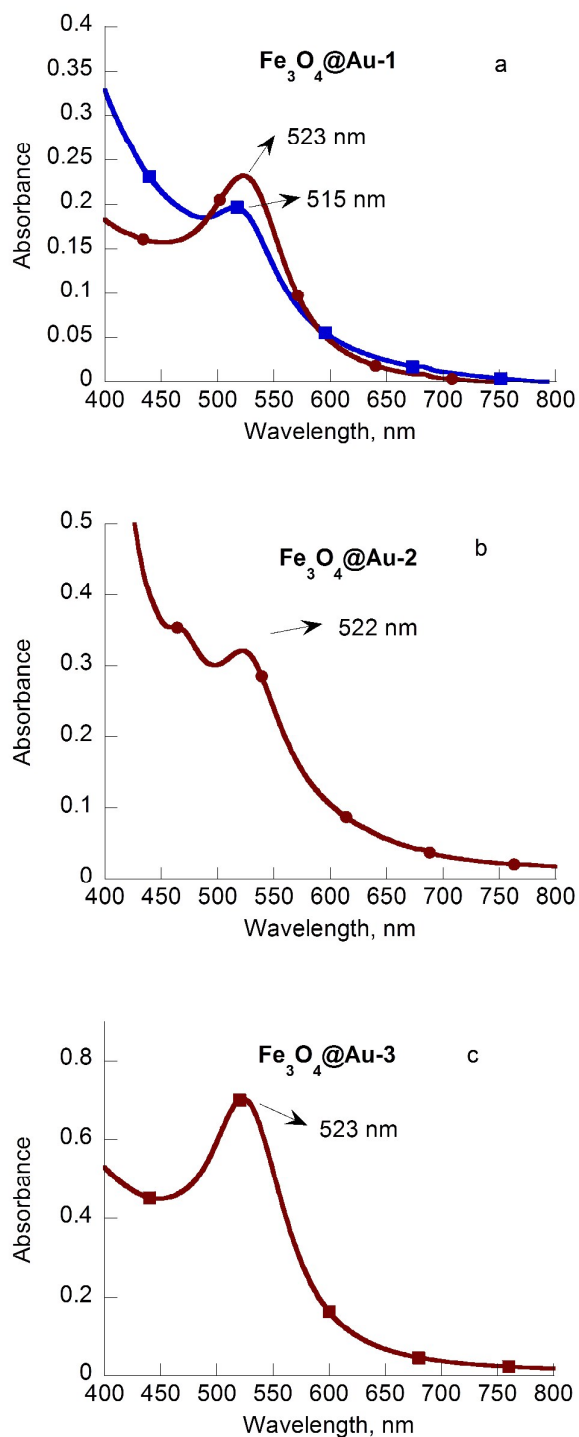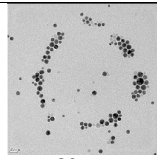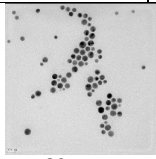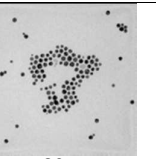
Nanoscale Accepted Manuscript

Journal Name

ARTICLE
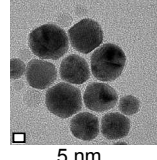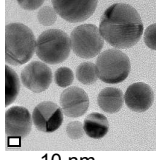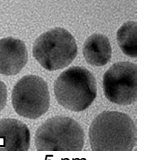
Figure 1: UV-visible spectra of toluene dispersions of Fe₃O₄@Au-1 (first precipitate in red, second precipitate in blue), b) Fe₃O₄@Au-2 and c) Fe₃O₄@Au-3.

Table 1 shows the HRTEM images of Fe₃O₄@Au-1, Fe₃O₄@Au-2 and Fe₃O₄@Au-3. They were recorded to check the size, crystallinity, and effectiveness in the shell formation (in the case of Fe₃O₄@Au-1 the images shown correspond to the first precipitate).

Nanometre-sized material was observed in all the cases. Images of Fe₃O₄@Au-1 NPs showed that the formation of the shell was not fully satisfactory and some uncovered Fe₃O₄ NPs were detected. This is in agreement with previous preparations of Fe₃O₄@Au NPs using Au(OOCCH₃)₃ as the gold salt, where a further separation by centrifugation was needed to obtain the desired core-shell Fe₃O₄@Au NPs (10.4 ± 2.3 nm).[23] In the case of Fe₃O₄@Au-2, two populations of NPs (of 15.9 ± 2.5 nm nm and 10.2 ± 2.1 nm) were observed; attempts to separate them by centrifugation were fruitless.

Table 1: HRTEM images of the core-shell **Fe₃O₄@Au NPs** using different gold precursors.

NP	**Fe₃O₄@Au-1** Au(OOCCH₃)₃	**Fe₃O₄@Au-2** HAuCl₄	**Fe₃O₄@Au-3** AuCl
Scale bar	20 nm	20 nm	20 nm
Scale bar	5 nm	10 nm	5 nm
Size	10.4 ± 2.3 nm	15.9 ± 2.5 nm 10.2 ± 2.1 nm	10.5 ± 1.5 nm

Remarkably, Fe₃O₄@Au-3 images showed a very homogeneous sample of core-shell Fe₃O₄@Au NPs with a diameter of 10.5 ± 1.5 nm (basically no Fe₃O₄ NPs were observed). These data demonstrate the crucial role of the gold salt for the successful formation of the metal shell on the Fe₃O₄ surface. Considering the size of the Fe₃O₄ NPs (5.0 ± 0.2 nm), we estimated the Au shell thickness as 2.8 ± 0.5 nm.

Regarding to the reproducibility of the preparation of Fe₃O₄@Au core-shell NPs, the use of freshly prepared magnetic NPs is crucial, since otherwise large NPs with a diameter of ca. 30 nm together with triangular-shaped NPs were formed over time. Furthermore, increasing the reflux temperature up to 265 °C produced two NP populations of 17 nm and 50 nm.

Fe₃O₄@Au-3 core-shell NPs characterisation

A twofold scale-up of the preparation of Fe₃O₄@Au-3 NPs was performed for the NP characterisation. In addition, the formation of the Au-shell on the magnetic NP surface was followed by HRTEM (Table S1). At short reaction times (1-5 minutes) most of the Fe₃O₄ NPs (ca. 70 %) were uncovered and the average diameter of the gold-covered NPs was of 8.9 ±0.9 nm. This value increased with the reaction

time reaching 9.3 ± 1.5 nm average size at 90 min, after which most of the NPs were core-shell NPs. In addition, a narrowing of the surface plasmon band was observed as the reaction time increase, almost preserving the same absorption maximum (521 nm).

The energy dispersive X-ray (EDX) spectrum showed the presence of intense peaks corresponding to Au together with low intense peak for Fe (Figure S2). The comparison between the EDX spectrum of an isolated core-shell Fe@Au nanoparticle recorded with the electron beam traversing the particle through both the shell and the core, and that recorded only traversing the shell, has been reported. In the latter case, the signal from Fe was undetectable. This can explain why the EDX spectrum of our core-shell Fe@Au nanoparticles does not reflect the real Au/Fe ratio.[28-29]

It is well known that dark-field microscopy collects only light that has been scattered obliquely by the sample.[30] Metallic NPs usually have strong scattering associated with the surface plasmon band. Indeed, optical dark-field images of the Fe_3O_4@Au-3 NPs showed the presence of bright spots corresponding to the presence of Au shell formed on the magnetic core Fe_3O_4 NPs surface (Figure 2a-b).
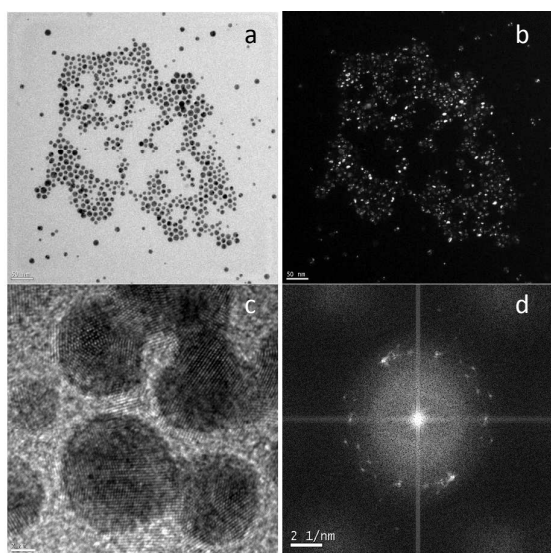

Figure 2: HRTEM image of Fe_3O_4@Au-3; scale bar of 50 nm (a) and 2 nm (c); dark field images (b) and FFT pattern (d) of Fe_3O_4@Au-3.

A close inspection of the electron diffraction (Figure 2d) of the NPs in Figure 2c indicates the presence of the characteristic diffraction planes (111 and 200) for cubic gold (JCPDS 00-004-0784). These data are in agreement with the diffraction peaks obtained in the PXRD spectrum for the Fe_3O_4@Au-3 NPs (Figure S3). In addition, the (220) and (331) peaks were also observed in the PXRD spectrum. It is noteworthy that these planes mainly correspond to the gold shell, consistent with a good gold covering of the magnetic NP.

Quantification of the inorganic content in the Fe_3O_4@Au-3 core-shell NPs was carried out by ICP-mass. The mass

percent of Fe found in the core-shell NPs was 32 ± 2 % compared to 5.2 ± 0.5 % for Au which correspond to the 0.57 and 0.026 for the atomic mass of Fe and Au in the sample, respectively.

The content of organic ligands in the Fe_3O_4@Au-3 NPs was analysed by thermogravimetry. The peak of the first derivative indicates the point of greatest rate change on the weight loss curve. For comparative purposes, the data were compared with those for Fe_3O_4 NPs.

The thermogravimetry analysis (TGA) of Fe_3O_4 (Figure S4) showed a weight loss of ca. 15.0% before reaching 350 ^{0}C (first derivative peak at 283 ^{0}C), which can be ascribed to the loss of the organic ligands present on the NP surface, such as oleic acid and oleylamine (see Figure S5 for the TGA heating curves of the ligands). In the case of Fe_3O_4@Au-3 core-shell NPs, the sample lost 15% weight before reaching 300 ^{0}C, followed by a weight loss of ca. 22% before reaching 450 ^{0}C with a 1st derivative peak at 230 ^{0}C and 425 ^{0}C, respectively. The latter might be ascribed to ligands on the gold surface with higher affinity to metallic surface than to the magnetic one.[31] The rest of the mass that did not decompose or sublimate at temperatures above 450 ^{0}C (85 % and 63 % for Fe_3O_4 and Fe_3O_4@Au-3 core-shell NPs, respectively) corresponds to the inorganic component of the NPs.

The magnetic studies on Fe_3O_4@Au NPs and Fe_3O_4 NPs revealed a decrease in the susceptibility, temperature blocking and magnetisation together with an increase in the coercivities in the case of the gold coated NPs. This is consistent with the coupling diminution of the magnetic moments as a result of the increased interparticle spacing of the magnetic cores, due to the gold shell in the case of Fe_3O_4@Au NPs (see Supporting information for more details and Figure S6-S7).[23]

Synthesis of the Fe_3O_4@Au@mSiO_2 nanoplatform

First, the Fe_3O_4@Au-3 NPs were transferred into an aqueous phase by using a cetyltrimethylammonium bromide (CTAB) aqueous solution to make them compatible with the reaction media to be incorporated into mSiO_2 NPs. Thus, the core-shell Fe_3O_4@Au-3 NPs dispersed in chloroform were mixed with an equal volume of CTAB (0.1 M in water) and the mixture was stirred until a homogeneous emulsion was formed. Chloroform evaporation under mild conditions induced the interaction between the hydrophobic chains of the organic ligands of the NP and those of CTAB. The absorption spectrum of the water dispersion of the Fe_3O_4@Au-3 NPs exhibited an SPB at ca. 532 nm (Figure S8), i.e., red-shifted compared to that of the NPs dispersed in organic media (SPB at ca. 521 nm) due to the higher polarity of water (the sensitivity of the localised surface plasmon band to the refractive index of the medium is well known).[32] [33].

The synthesis of mSiO_2 NPs was carried out by using a previous described methodology with some modification (see details in the experimental section).[7] The preparation consists in three main steps; i) synthesis, ii) purification and

Journal Name **ARTICLE**

iii) template removal. Briefly, the synthesis of mSiO$_2$ NPs was performed using CTAB, as directing agent to produce hexagonal arrangement in the silica (MCM-41), tetraethyl orthosilicate (TEOS), NH$_4$OH and ethyl acetate. The purification of the NPs was carried out by several washing-centrifugation cycles using ethanol and water as solvents. Then, a solution of NH$_4$NO$_3$ was used for the removal of the organic template to clean the internal pores of the mSiO$_2$. Different NH$_4$NO$_3$ concentrations were evaluated (0.03-0.06 mg/mL) and it was observed that the highest concentration was the best condition for total CTAB removal. Finally the solid obtained was dispersed in water.

Empty channels were clearly observed in the HRTEM images mSiO$_2$ NPs (Figure S9). In fact, TGA analysis confirmed the complete elimination of the template under these conditions.[34] The silica NPs presented a size of 97 ± 6 nm, which was confirmed by HRTEM and SEM (Figure S9).

Encapsulation of Fe$_3$O$_4$@Au-3 NPs capped with CTAB into mSiO$_2$ was optimised with the aim of incorporating mostly one core-shell NP by Fe$_3$O$_4$@Au@mSiO$_2$ NPT while preserving the spherical shape and nanoscale regime (below 100 nm) of the final system. Different factors such as magnetic stirring, reaction time and concentration of the core-shell NPs were evaluated.

The reproducibility of the synthesis was improved using an orbital shaker, instead of magnetic stirring. Different agitation times were evaluated from 30 to 90 minutes, and the more homogeneous size of the NPT was obtained at 60 minutes in the orbital shaker (450 rpm). Under the optimal conditions, different core-shell NP concentrations were studied (10-40 μL of the 45 mg/mL concentrated NPs dispersed in CTAB) keeping constant the total amount of CTAB (0.0275 mmol). The resulting Fe$_3$O$_4$@Au@mSiO$_2$ NPT was analysed by TEM microscopy (Figure 3a). The best results, in terms of the homogeneity of the nanoplatform shape, as well as the distribution of the Fe$_3$O$_4$@Au-3 NPs into the silica, were obtained when using 20 μL of the Fe$_3$O$_4$@Au-3 NPs capped with CTAB.

A large scale synthesis (increasing the quantities ten times) carried out under the optimal conditions led to 60 ± 5 nm-sized spherical NPT. The presence of Fe$_3$O$_4$@Au-3 NPs inside the NPT was clearly observed by TEM as dark nanoparticles (Figure 3a). Mostly one Fe$_3$O$_4$@Au-3 NP was present in the silica matrix of each NPT and they were clearly located close to an edge of the mSiO$_2$ matrix.

Previous studies have reported on the structure evolution of mesoporous silica nanoparticles incorporating small magnetic nanoparticles. The small magnetic Fe$_3$O$_4$ nanoparticles retarded the crystallization of the mesoporous silica and eventually the Fe$_3$O$_4$ nanoparticles relocated towards the particle edge acting as an impurity[7]. Thus, the small Fe$_3$O$_4$@Au nanoparticles could also act as impurities leading to the same result. Control experiments of the incorporation of 9 nm-sized AuNPs[35] and 5 nm-sized Fe$_3$O$_4$ NPs into mSiO$_2$ NPs were performed under the above-mentioned conditions. These assays showed that while the

AuNPs located in the centre of the silica, thus leading to symmetrical Au@mSiO$_2$ NPs of 66 ± 6 nm, the magnetic NPs located near the outer surface of the mSiO$_2$ in the Fe$_3$O$_4$@mSiO$_2$ NPs of 50 ± 5 nm (Figure S10). These results are consistent with those previously reported for small iron oxide NPs embedded in ordered mSiO$_2$ NPs[7] and reveal that the thin Au-shell does not affect the trend of Fe$_3$O$_4$ to be placed at an edge of the silica matrix surface.
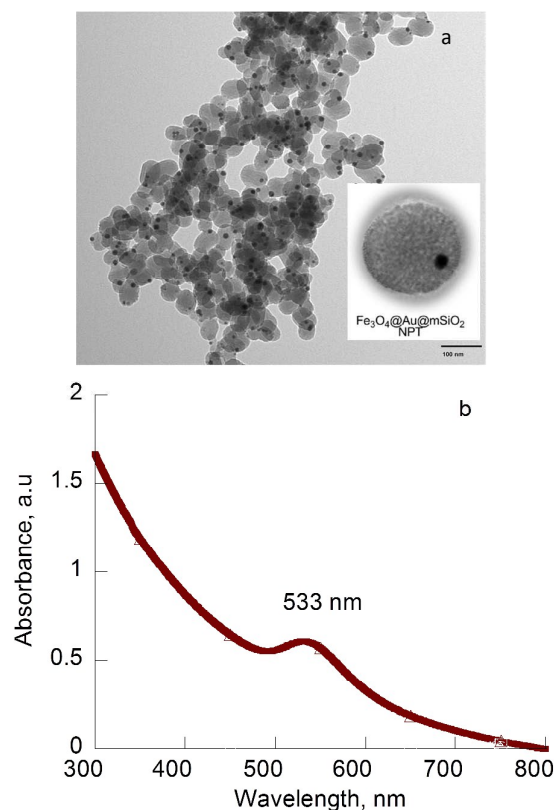
Figure 3: a) TEM image of the Fe$_3$O$_4$@Au@mSiO$_2$ nanoplataform (scale bar = 100 nm), and b) UV-visible absorption spectrum of Fe$_3$O$_4$@Au@mSiO$_2$ nanoplataform in water. Inset in Figure 1a: TEM image of an individual NPT.

Regarding the optical properties of the NPT, the spectrum showed the SPB peak of the Fe$_3$O$_4$@Au@mSiO$_2$ NPT at ca. 533 nm in water (this value is similar to that found for Fe$_3$O$_4$@Au NPs in water), Figure 3b.

Covalent binding of RB to the nanoplatform pores

To bind RB firmly to the inner walls of the NPT, they were first functionalised with amino groups by reacting the silanol groups with (3-aminopropyl)triethoxysilane (APTES) in toluene at 120 ^{0}C for 5 h (see experimental section for details).[36] Then, the conjugation of RB to the functionalised pores was carried out in methanol at room temperature overnight, using 1-etil-3-(3-dimetilaminopropil)carbodiimida (EDC) as a coupling agent leading to NPT-RB (Scheme 2).

ARTICLE   **Journal Name**
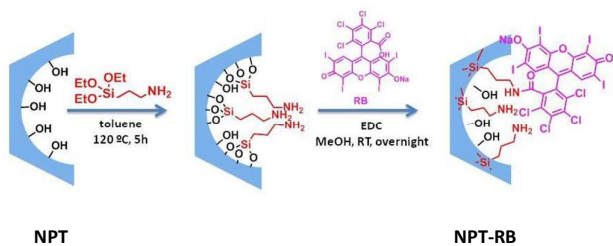
Scheme 2: General procedure for the functionalisation of the Fe_3O_4@Au@mSiO$_2$ nanoplatform (NPT) with Rose Bengal (RB).

It is known that the λ_{max} value of the RB absorption spectrum strongly depends on the medium. Thus, in water the peak of RB has been reported at 546 nm as is the case of mSiO$_2$@RB NPs in which the RB units are at the NP periphery.[37] However, the peak of RB-encapsulated into mSiO$_2$ NPs (mSiO$_2$-RB) shifts to ca. 564 nm.[20] Consequently, the red shift is attributed to confinement effects combined with the different chemical environment inside the pores. The absorption spectrum of Fe_3O_4@Au@mSiO$_2$-RB in water (Figure 4) exhibited a peak at 570 nm, i.e., slightly shifted to longer wavelengths compared to mSiO$_2$-RB, indicating the successful functionalisation of the silica pores with RB.

With respect to the emission, SiO$_2$@RB NPs show a peak at 568 nm, like free RB does (Figure S11). However, the emission peak of the RB monomer in the nanosystems shifts to the red (at ca. 580 nm).

It is known that large particles scatter a fraction of light and hence it is expected that the RB absorption in mSiO$_2$-RB, Fe_3O_4@mSiO$_2$-RB, and Fe_3O_4@Au@mSiO$_2$-RB be less efficient than in RB.

The FTIR spectra of RB, Fe_3O_4@Au@m-SiO$_2$-RB, and m-SiO$_2$-NH$_2$ is shown in Figure S12. The spectrum of Fe_3O_4@Au@m-SiO$_2$-RB shows bands located at similar wavenumbers to those ascribed to the covalent coupling of RB to SiO$_2$.[38-39]
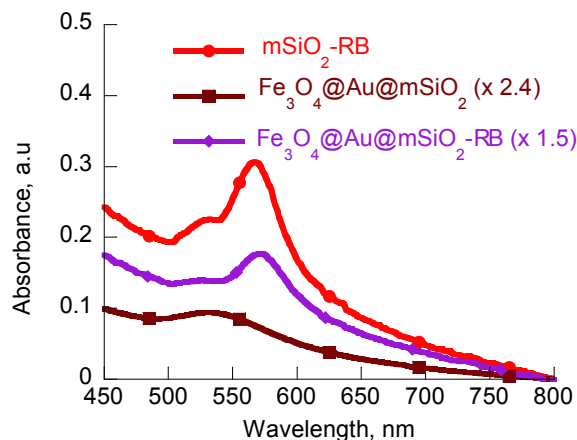

Figure 4: Comparison between the absorption spectra in water of Fe_3O_4@Au@mSiO$_2$-RB (in violet), Fe_3O_4@Au@mSiO$_2$ (in dark red) and mSiO$_2$-RB (in red).

Singlet oxygen formation studies

An excited photosensitiser located near a AuNP (an optical antenna) functions as a transmitter and, similarly, a photosensitiser in its ground state excited by the localised field near the optical antenna acts as a receiver.[40] Singlet oxygen ($^1O_2$) generation is related to the photosensitiser triplet quantum yield and this can be increased by surface plasmon sensitisation due to antenna effects.[41-43] A match between the SPB energy and the excitation energy of the photosensitiser, as well as the closeness between the photosensitiser and the metal NP, are required for maximising the enhancement.[44]

There are two main methods to measure the capacity of a photosensitiser to generate singlet oxygen ($^1O_2$): i) direct measurement of the characteristic phosphorescence spectrum of $^1O_2$ (λ_{max} = 1270 nm) and ii) indirect techniques using a chemical probe such as 9,10-anthracenediyl-bis(methylene)dimalonic acid (ABDA). The probe reacts irreversibly with $^1O_2$ generated by photoexcitation of the photosensitiser and the reaction can be followed spectrophotometrically by recording the absorption decrease of the chemical probe at a given wavelength.[45] The latter method was employed in our case, since it is easy to follow the absorption signal of ABDA during irradiation times.
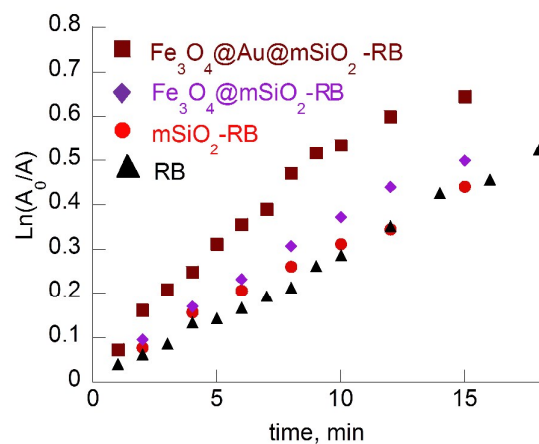
Figure 5: Plot of Ln (A$_0$/A) vs irradiation time for water dispersions of RB (black), mSiO$_2$-RB (red), Fe_3O_4@mSiO$_2$-RB (violet) and Fe_3O_4@Au@mSiO$_2$-RB (dark red) in the presence of ABDA; absorbance of ABDA measured at 380 nm where it has a strong absorption.

The efficiency of Fe_3O_4@Au@mSiO$_2$-RB water dispersions in singlet oxygen generation was evaluated by using ABDA as a probe and it was compared with those of the analogous-sized mSiO$_2$-RB and Fe_3O_4@mSiO$_2$-RB nanosystems as well as with that of RB (see Figure S13 and Figure S14 for RB and Fe_3O_4@Au@mSiO$_2$-RB). The RB absorbance of all the samples was fixed at approximately 0.15 and the probe (20 μM) was added to each sample. Then, the samples were irradiated for up to 15 minutes inside a photoreactor equipped with eight visible lamps (530-700 nm wavelength range, maximum ca. 580 nm). The absorbance changes at 380 nm, where ABDA shows a strong absorption, were

plotted vs the time of irradiation. Figure 5 compares the efficiency of the nanosystems and shows that $Fe_3O_4@Au@mSiO_2$-RB was the most efficient.

The similar efficiency of RB and $mSiO_2$-RB is a good agreement with previous results.[20]

Therefore, taking into account that all the samples contained the same amount of RB, the 1.5-fold enhancement in the degradation of ABDA by $Fe_3O_4@Au@mSiO_2$-RB can be attributed to surface plasmon sensitisation. Laser flash photolysis (λ_{exc}=532 nm) of $Fe_3O_4@Au@mSiO_2$-RB and RB, both samples with the same absorbance at the excitation wavelength, corroborated the enhanced yield of the Rose Bengal triplet (^{3}RB) in the nanoplatform compared with that of free Rose Bengal (see further details in the Experimental Section and Figures S15-17).

Experimental

Chemicals. All reagents were commercially available and used as received. Iron (III) acetylacetonate (Fe(acac)3, 99.9%), 1,2- hexadecanediol ($C_{14}H_{29}CH(OH)CH_2(OH)$, 90%), oleylamine (OAM, C_9H_{18}=$C_9H_{17}NH_2$, 70%), oleic acid (OA, C_9H_{18}=C_8H_{15}- COOH, 99%), phenyl ether ($C_{12}H_{10}O$, 99%) and other solvents (hexane, ethanol and chloroform) were purchased from Sigma–Aldrich. Gold acetate Au(OOCCH₃)₃, or Au(ac)₃, 99.9%) and AuCl (99.99%) were purchased from Sigma-Aldrich.

Hexadecyltrimethylammonium bromide (CTAB, ≥ 98%), ethyl acetate (99.8 %), tetraethyl orthosilicate (TEOS, ≥ 99%, GC), ammonium hydroxide (28%), acetic acid (glacial), ethanol (absolute, anhydrous), deionized water (Milli-Q), ammonium nitrate (≥ 99%) and chloroform (≥ 99%) were purchased from Sigma-Aldrich and used as obtained without further purification.

Rose Bengal, 3-aminopropyl-triethoxysilane (APTES), toluene, and 1-ethyl-3-(3-dimethylaminopropyl) carbodiimide-HCl (EDC) were purchased from Sigma-Aldrich.

Absorption measurements. UV-vis spectra were recorded at room temperature using a quartz cuvettes spectrometer in a UV-visible spectrophotometer Agilent 8453E.

Irradiation experiments. Samples were irradiated in 10x10 mm quartz cuvettes in a Luzchem photoreactor equipped with eight visible lamps (380-490 nm, maximum at 419 nm with a dose 70.02 Wm^{-2} in the 401-700 nm range).

ICP-OES Analysis. The iron and gold content in the core-shell $Fe_3O_4@Au$ nanoparticle was measured by ICP-OES analysis. The samples were prepared by acid digestion in a microwave oven at high pressure. The concentration ranges of the dilutions from the digested solution were optimized in order to provide reproducible and comparable results compatible with the sensitivity of the analytical methods employed.

Thermogravimetry analyses. The analyses of the samples were carried out with a Mettler Toledo TGA/SDTA 851 apparatus in the 25-800 ºC temperature range under a 10 ºC.min⁻¹ scan rate and an air flow of 30 mL/min⁻¹.

FTIR Measurements. The FTIR spectra were collected on a Fourier Transformation-Infrared Spectrometer NICOLET 5700, using KBr pellets in the frecuency range 3000-500 cm⁻¹.

Magnetic Measurements. All the magnetic measurements were carried out with a magnetometer using powdered samples (Quantum Design MPMS-XL-5) equipped with a SQUID sensor. Variable temperature susceptibility measurements were carried out on powdered samples in the 2-300 K range at magnetic fields of 10 Oe. The diamagnetism from the holder was corrected by measuring the empty holder at the same conditions (magnetic field and temperature) used for the measurement of the NPs. Diamagnetism from the NPs was also corrected taking into account the amount of capping agent and solvent surrounding the NPs derived from thermal analysis. The hysteresis studies were performed between 5 and -5 T, at 5 K, cooling the samples at zero fields.

Synthesis of Fe_3O_4 nanoparticles. Fe_3O_4 NPs were synthesised using a previously described protocol reported in the literature with some modification. Under argon atmosphere and vigorous stirring, 0.71 g Fe(acac)₃ (2 mmol) were poured in 20 mL of phenyl ether with 2 mL of oleic acid (6 mmol) and 2 mL of oleylamine (4 mmol). Then, 2.58 g of 1,2-hexadecanediol (10 mmol) was added into the solution. The reaction solution was heated to 210 °C and refluxed at 265 °C for 2 hours. After cooling to room temperature, part of the solution (5 mL) was centrifuge twice in ethanol to further characterisation (16 mg/mL) and the crude of the reaction was used for the synthesis of core-shell NPs.

Synthesis of $Fe_3O_4@Au$. For $Fe_3O_4@Au$ NPs synthesis, three different gold precursors (Au(OOCCH₃)₃, HAuCl₄ and AuCl were used.

Synthesis of $Fe_3O_4@Au(1)$. 5 mL of the Fe_3O_4 crude solution (0.165 mmol Fe_3O_4), 0.41 g (1.1 mmol) of Au(OOCCH₃)₃, 1.55 g (6 mmol) of 1,2-hexadecanediol, 0.25 mL (0.75 mmol) of oleic acid, 1.5 mL (3 mmol) of oleylamine were added into 15 mL of phenyl ether. The molar ratio of the Au precursor to the iron oxide NPs was approximately 7:1. The reaction was heated to 180-190 °C at 10°C/min for 1.5 hours, under argon atmosphere and vigorous stirring. After cooling to room temperature, 40 mL of ethanol were added into the solution. A dark-purple material was separated by centrifugation at 7000 rpm during 20 minutes. The precipitated product was washed with ethanol. The precipitate was redispersed in 5 mL of chloroform in the presence of ca. 75 mM of oleic acid and oleylamine and the NP dispersion was dark purple. An aliquote (200 μL) of the NPs were diluted into 6 mL of chloroform.

Synthesis of $Fe_3O_4@Au-2$. The synthesis method was carried out following the same procedure than for $Fe_3O_4@Au-1$ except the gold precursor was but HAuCl₄ 0.433 g (1.1 mmol).

Synthesis of $Fe_3O_4@Au-3$. The synthesis method was carried out following the same procedure than for

Fe$_3$O$_4$@Au-1 except the gold precursor was AuCl 0.257 g (1.1 mmol). The core-shell NPs obtained (407 mg) was dispersed in 5 mL chloroform.

Synthesis of mSiO$_2$ nanoparticles. Mesoporous silica NPs were synthesised as control NPs. The synthesis was performed using a modified protocol from Suteewong *et al.*[7] CTAB solution (500 µL of 55 mM) were diluted in 10 mL of water, followed by the addition of 0.088 mL of ethyl acetate, 0.27 mL of NH$_4$OH 28 % and finally 50 µL TEOS. The solution was stirred for 5 minutes at 450 rpm in an orbital shaker. Afterwards, 3.7 mL of water was added into the reaction and stirred for 1 hour at 450 rpm in an orbital shaker.

The purification process consisted in the neutralisation of the reaction solution with acetic acid 1.6 M and then washing with ethanol and water by centrifugation at 9000rpm during 15 minutes.

The surfactant templates were subsequently removed under sonication of the resulting solution with 25 mL ammonium nitrate (0.66 mg/mL) in ethanol during 40 minutes and a subsequent centrifugation with ethanol, ethanol:water (1:1) and water at 9000rpm for 15 minutes.

Synthesis of Fe$_3$O$_4$@Au-mSiO$_2$. The synthesis of the Fe$_3$O$_4$@Au@mSiO$_2$-RB nanosystem was performed using the same procedure to that described above. Optimization parameters are summarized in Table S2. The best results were obtained using an aliquot (20 µL) of Fe$_3$O$_4$@Au NPs (22 mg/mL) and 464 µL of CTAB 55 mM (thus a total of 0.0275 mmol of CTAB), which were diluted in 10 mL of water. This was followed by the addition of 0.088 mL of ethyl acetate, 0.27 mL of NH$_4$OH 28 % and 50 µL TEOS. The solution was stirred for 5 minutes at 450 rpm. Afterwards, 3.7 mL of water was added into the reaction and stirred for 1 hour at 450 rpm. The purification steps and template removal were the same as those described above.

Functionalisation of Fe$_3$O$_4$@Au-mSiO$_2$. The pores of the NPT were functionalised with Rose Bengal. The first step was the derivatisation of the alcohol groups with (3-aminopropyl)triethoxysilane (APTES). Briefly 55 mg of Fe$_3$O$_4$@Au@mSiO$_2$ were mixed with toluene and heated for 30 minutes at 50 ^{0}C. Then, APTES (0.39 mmol) and *p*-toluene sulphonic acid (PSTA, 0.013 mmol) were added and heated up to 120 ^{0}C during 5 hours. The reaction was cooled down to room temperature and poured into a centrifuge tube, followed by the addition of 21 mL of ethanol. It was centrifuged at 10.000 rpm for 20 minutes at 20 ^{0}C, and washed with ethanol under the same conditions. Previous to the centrifugation, the sample was sonicated during 2-3 minutes. Finally the solid (40 mg) was dispersed into acetone and dry to vacuum. The amine-NPT was mixed with Rose Bengal (0.037 mmol) in 1.2 mL of pyridine in the presence of 1-ethyl-3-(3-dimethylaminopropyl) carbodiimide (EDC, 0.15 mmol) and the mixture was stirred overnight and then quenched with 8 mL of water to deactivate the unreactive EDC. The mixture was washed six times with ethanol (7 mL) and centrifuged at 9.000 rpm for 10 minutes at 20 ^{0}C. The pH of the solution was lowered

until 1-2 with HCl and centrifuged twice and then it was washed with NaHCO$_3$ and ethanol. The final solid was re-dispersed in acetone (5 mL) and dried in vacuum (48.9 mg).

Singlet oxygen formation studies. A solution of RB (2.9 µM) in water was prepared and 3mL were transferred in a cuvette. Then 200 µL of ABDA were added and the spectrum was register between 400-700 nm (time 0). The sample was irradiated in a photoreactor using visible lamps (530-570 nm). The absorption spectra were registered every 10 minutes during 60 minutes.

Laser flash photolysis measurements

Laser flash photolysis measurements were carried out using a Nd:YAG laser (λ_{exc} = 532 nm) with a pulse width of 5-8 ns and power of 10.7 mW. The output signal from the oscilloscope was transferred to a personal computer.

An acetonitrile dispersion of the nanoplatform (2 mg) was freshly prepared and sonicated for 5 minutes. The dispersion was transferred into a quartz cuvette and purged with nitrogen for 7 minutes. The absorption spectrum of the NPT was measured and Figure S15a (blue line) showed the high contribution of the scattering to the total spectrum. In order to calculate the scattering contribution (y_{sc}), the data from the original spectrum between 467 nm and 497 nm, and 687 nm and 800 nm were fitted to a second-degree polynomial function ($y_{sc} = A\lambda^2 + B\lambda + C$) and the R-square observed was 0.9997. The quadratic (A), linear (B) and independent (C) coefficients were $3.18\pm0.02\times10^{-6}$, $-5.96\pm0.03\times10^{-3}$ and 3.255 ± 0.009, respectively. The corrected absorption spectrum of the NPT (Figure S15 a, brown line) was obtained by subtraction of the scattering contribution to the original spectrum. The absorbance of the Rose Bengal in NPT was 0.18 at 532 nm. For comparative purpose, a Rose Bengal solution with the same absorbance at 532 nm was also prepared (Figure S15 b). No changes in the absorption spectrum of Fe$_3$O$_4$@Au@mSiO$_2$-RB were observed after 532 nm laser exposure (spectra not shown).

Conclusion

We have successfully prepared a novel Fe$_3$O$_4$@Au@mSiO$_2$ nanoplatform in which mainly just one Fe$_3$O$_4$@Au nanoparticle is embedded and which is near the outer surface of the mSiO$_2$ matrix. Covalent binding of the therapeutic drug, namely Rose Bengal, to the silica pores led to the Fe$_3$O$_4$@Au@mSiO$_2$-RB nanophotosensitiser, whose efficiency in singlet oxygen generation was about 1.5-times higher than that of analogous-sized mSiO$_2$-RB and Fe$_3$O$_4$@mSiO$_2$-RB nanosystems.

This enhancement can be attributed to surface plasmon sensitisation and is remarkable because of the small size of the plasmonic component in the matrix. This is a new way of embedding an antenna in a matrix. If we take into account the trend of the magnetic NPs to accumulate in the same area, the further potential for singlet oxygen enhancement by using Fe$_3$O$_4$@Au@mSiO$_2$ nanoplatforms containing several Fe$_3$O$_4$@Au NPs in each silica matrix is worth studying and will be addressed in due course.

Journal Name

ARTICLE

Acknowledgements

Notes and references

1   1.   L. Ricciardi, M. Martini, O. Tillement, L. Sancey, P. Perriat, M. Ghedini, E. I. Szerb, Y. J. Yadav and M. La Deda, *Journal of Photochemistry and Photobiology B: Biology*, 2014, **140**, 396-404.

2   2.   J. Zheng, Y. Dong, W. Wang, Y. Ma, J. Hu, X. Chen and X. Chen, *Nanoscale*, 2013, **5**, 4894-4901.

3   3.   H. Liu, C. Lin, Z. Ma, H. Yu and S. Zhou, *Molecules*, 2013, **18**, 14258.

4   4.   J. Yang, D. Shen, L. Zhou, W. Li, X. Li, C. Yao, R. Wang, A. M. El-Toni, F. Zhang and D. Zhao, *Chemistry of Materials*, 2013, **25**, 3030-3037.

5   5.   T.-H. Tran and T.-D. Nguyen, *Functional Inorganic Nanohybrids for Biomedical Diagnosis*, 2013.

6   6.   Z. Liu, L. Sun, F. Li, Q. Liu, L. Shi, D. Zhang, S. Yuan, T. Liu and Y. Qiu, *Journal of Materials Chemistry*, 2011, **21**, 17615-17618.

7   7.   T. Suteewong, H. Sai, J. Lee, M. Bradbury, T. Hyeon, S. M. Gruner and U. Wiesner, *Journal of Materials Chemistry*, 2010, **20**, 7807-7814.

8   8.   M. K. Yu, Y. Y. Jeong, J. Park, S. Park, J. W. Kim, J. J. Min, K. Kim and S. Jon, *Angewandte Chemie International Edition*, 2008, **47**, 5362-5365.

9   9.   S. Kayal and R. V. Ramanujan, *Journal of Nanoscience and Nanotechnology*, 2010, **10**, 5527-5539.

10   10.   A.-H. Lu, E. L. Salabas and F. Schüth, *Angewandte Chemie International Edition*, 2007, **46**, 1222-1244.

11   11.   X. He, L. Tan, D. Chen, X. Wu, X. Ren, Y. Zhang, X. Meng and F. Tang, *Chemical Communications*, 2013, **49**, 4643-4645.

12   12.   F. Tang, L. Li and D. Chen, *Advanced Materials*, 2012, **24**, 1504-1534.

13   13.   P. Yang, S. Gai and J. Lin, *Chemical Society Reviews*, 2012, **41**, 3679-3698.

14   14.   R. K. Lansche, *American Journal of Ophthalmology*, 1965, **60**, 520-525.

15   15.   S. Tsao, M. Yao, H. Tsao, F. P. Henry, Y. Zhao, J. J. Kochevar, R. W. Redmond and I. E. Kochevar, *British Journal of Dermatology*, 2012, **166**, 555-563.

16   16.   A. Ormond and H. Freeman, *Materials*, 2013, **6**, 817.

17   17.   G. R. Fleming, A. W. E. Knight, J. M. Morris, R. J. S. Morrison and G. W. Robinson, *Journal of the American Chemical Society*, 1977, **99**, 4306-4311.

18   18.   L. Ludvikova, P. Fris, D. Heger, P. Sebej, J. Wirz and P. Klan, *Physical Chemistry Chemical Physics*, 2016, **18**, 16266-16273.

19   19.   E. Gandin, Y. Lion and A. Van de Vorst, *Photochemistry and Photobiology*, 1983, **37**, 271-278.

20   20.   E. Gianotti, B. Martins Estevão, F. Cucinotta, N. Hioka, M. Rizzi, F. Renò and L. Marchese, *Chemistry – A European Journal*, 2014, **20**, 10921-10925.

21   21.   This effect has also been observed for other photosensitizers`, such as riboflavin`, see reference 19.

22   22.   N. C. Angeluzzi, M. Munoz, D. T. Marquez, M. S. Baptista, A. M. Edwards, E. I. Alarcon and J. C. Scaiano, *Journal of Materials Chemistry B*, 2014, **2**, 4221-4225.

23   23.   WangWang, J. Luo, Q. Fan, M. Suzuki, I. S. Suzuki, M. H. Engelhard, Y. Lin, N. Kim, J. Q. Wang and C.-J. Zhong, *The Journal of Physical Chemistry B*, 2005, **109**, 21593-21601.

24   24.   Under the same experimental conditions but in the absence of the Fe3O4 NP a heterogeneous sample containing gold particles from fifty to a few hundred nm were obtained.

25   25.   W. K. Mark and J. H. Naomi, *New Journal of Physics*, 2008, **10**, 105006.

26   26.   C. S. S. R. Kumar, in *Mixed Metal Nanomaterials* Weinheim: Wiley-VCH, 2009.

27   27.   P. K. Jain and M. A. El-Sayed, *Nano letters*, 2007, **7**, 2854-2858.

28   28.   J. Zhang, M. Post, T. Veres, Z. J. Jakubek, J. Guan, D. Wang, F. Normandin, Y. Deslandes and B. Simard, *The Journal of Physical Chemistry B*, 2006, **110**, 7122-7128.

29   29.   C. Langlois, P. Benzo, R. Arenal, M. Benoit, J. Nicolai, N. Combe, A. Ponchet and M. J. Casanove, *Nano letters*, 2015, **15**, 5075-5080.

30   30.   E. Ringe, B. Sharma, A.-I. Henry, L. D. Marks and R. P. Van Duyne, *Physical Chemistry Chemical Physics*, 2013, **15**, 4110-4129.

31   31.   J. Manson, D. Kumar, B. J. Meenan and D. Dixon, *Gold Bulletin*, 2011, **44**, 99-105.

32   32.   F. Chen, Q. Chen, S. Fang, Y. a. Sun, Z. Chen, G. Xie and Y. Du, *Dalton Transactions*, 2011, **40**, 10857-10864.

33   33.   M. M. Miller and A. A. Lazarides, *The Journal of Physical Chemistry B*, 2005, **109**, 21556-21565.

34   34.   Removal of the template by calcination was avoided to keep the integrity of the nanoparticles

Nanoscale Accepted Manuscript

when preparing the Fe3O4`@Au`@mSiO2nanoplatform.

35   35.   H. Hiramatsu and F. E. Osterloh, *Chemistry of Materials*, 2004, **16**, 2509-2511.

36   36.   J. A. Bae, K.-C. Song, J.-K. Jeon, Y. S. Ko, Y.-K. Park and J.-H. Yim, *Microporous and Mesoporous Materials*, 2009, **123**, 289-297.

37   37.   Y. Guo, S. Rogelj and P. Zhang, *Nanotechnology*, 2010, **21**, 065102-065102.

38   38.   B. Martins Estevao, F. Cucinotta, N. Hioka, M. Cossi, M. Argeri, G. Paul, L. Marchese and E. Gianotti, *Physical Chemistry Chemical Physics*, 2015, **17**, 26804-26812.

39   39.   A. Uppal, B. Jain, P. K. Gupta and K. Das, *Photochemistry and Photobiology*, 2011, **87**, 1146-1151.

40   40.   P. Bharadwaj and L. Novotny, *Opt. Express*, 2007, **15**, 14266-14274.

41   41.   N. L. Pacioni, M. González-Béjar, E. Alarcón, K. L. McGilvray and J. C. Scaiano, *Journal of the American Chemical Society*, 2010, **132**, 6298-6299.

42   42.   Y. Zhang, K. Aslan, M. J. R. Previte and C. D. Geddes, *Journal of Fluorescence*, 2007, **17**, 345-349.

43   43.   S. M. Mooi and B. Heyne, *Photochemistry and Photobiology*, 2014, **90**, 85-91.

44   44.   P. Wang, H. Tang and P. Zhang, *Scientific Reports*, 2016, **6**, 34981.

45   45.   M. C. DeRosa and R. J. Crutchley, *Coordination Chemistry Reviews*, 2002, **233–234**, 351-371.

46

Journal Name

ARTICLE

A novel nanoplatform integrated by a core-shell Fe_3O_4@Au nanoparticles encapsulated near the outer surface of $mSiO_2$ nanoparticles, has been successfully synthesised and proved to enhance the efficiency of Rose Bengal for singlet oxygen generation.

Nanoscale Accepted Manuscript

Please do not adjust margins